



## City Research Online

### City, University of London Institutional Repository

---

**Citation:** Tsavdaridis, K. D., D'Mello, C. & Huo, B. Y. (2013). Experimental and computational study of the vertical shear behaviour of partially encased perforated steel beams. *Engineering Structures*, 56, pp. 805-822. doi: 10.1016/j.engstruct.2013.04.025

This is the accepted version of the paper.

This version of the publication may differ from the final published version.

---

**Permanent repository link:** <https://openaccess.city.ac.uk/id/eprint/14017/>

**Link to published version:** <https://doi.org/10.1016/j.engstruct.2013.04.025>

**Copyright:** City Research Online aims to make research outputs of City, University of London available to a wider audience. Copyright and Moral Rights remain with the author(s) and/or copyright holders. URLs from City Research Online may be freely distributed and linked to.

**Reuse:** Copies of full items can be used for personal research or study, educational, or not-for-profit purposes without prior permission or charge. Provided that the authors, title and full bibliographic details are credited, a hyperlink and/or URL is given for the original metadata page and the content is not changed in any way.

---

---

---

City Research Online:

<http://openaccess.city.ac.uk/>

[publications@city.ac.uk](mailto:publications@city.ac.uk)

---

# EXPERIMENTAL AND COMPUTATIONAL STUDY OF THE VERTICAL SHEAR BEHAVIOUR OF PARTIALLY ENCASED PERFORATED STEEL BEAMS

Konstantinos Daniel Tsavdaridis<sup>1\*</sup>, Cedric D'Mello<sup>2</sup>

<sup>1</sup>*School of Engineering and Mathematical Sciences, City University London, EC1V 0HB, UK, Office: C354, E-mail: [konstantinos.tsavdaridis.2@city.ac.uk](mailto:konstantinos.tsavdaridis.2@city.ac.uk)*

<sup>2</sup>*School of Engineering and Mathematical Sciences, City University London, EC1V 0HB, UK, Office: C173, E-mail: [C.A.Dmello-1@city.ac.uk](mailto:C.A.Dmello-1@city.ac.uk)*

---

## 1. Introduction

Structures such as high-rise buildings, benefit from shallow flooring systems since the floor-to-floor height is a significant factor. The fact that a conventional composite beam is deeper than a reinforced concrete beam is a strong disadvantage. Hence, in several situations it is important to reduce the overall depth of the floor using partially encased composite beams [1]. These fully composite beams also have other advantages such as increased fire resistance, load carrying capacity, local buckling stiffness and dramatic increase in the bending stiffness compared to conventional beams. Moreover, a lower construction cost compared to the reinforced concrete or the steel frame systems is achieved by using partially encased composite beams eliminating the construction time and amount of formwork and scaffolding [2, 3, 4, 5].

Comparing conventional composite flooring systems and partially encased composite beams it is seen that the concrete between flanges in the latter case increases the bending stiffness and reduces the vertical displacements. Despite the advantages in terms of structural behaviour and cost, the behaviour of encased perforated beam is not entirely understood yet.

Whilst numerous research papers were found in the literature review regarding conventional composite flooring systems with the use of plane and perforated steel beams and partially encased composite beams with the use of plain steel sections, only recently has very limited study been carried out on partially encased composite beams with the use of perforated steel sections [1, 6, 7].





**Fig. 1:** USFB used with profiled steel decking (top) and with precast concrete unit (bottom) (adopted by [8])

## 2. New composite flooring system

For conventional composite floor beams or down stand composite beams, the thickness of the flanges increases with the increase in span. Consequently, the steel sections are often heavier than needed [9]. The Ultra Shallow Floor Beam (USFB), is a new type of composite floor beam, which is fabricated by welding two highly asymmetric cellular tee-sections together along the web. Profiled steel decking or precast concrete floor units sit on the bottom flange, as shown in **Fig. 1**. The top and bottom tee-sections are cut from different parent sections where the top tee is much smaller than the bottom tee. This asymmetric section property reduces the weight of the beam and also increases the moment capacity. The circular or elongated web openings provide a channel for reinforcing tie-bars, building services and ducting through the structural depth of the beam, thus minimising the overall floor depth. Transverse reinforcing tie-bars can provide longitudinal shear strength by tying the concrete on both sides of the web. Shear studs can be also used, welded horizontally on the web of the steel beams. Full service integration can be achieved when deep profiled steel decking is employed, as pipes or ducts pass through between the ribs of the steel decking. As the floors are cast, the in-situ concrete passes through the web openings, which may or may not include a tie-bar or duct. This concrete plug forms a unique mechanism for transferring longitudinal shear force along the beam. A special end diaphragm is used for deep decking floor applications so that the concrete fully surrounds the steel section, apart from the bottom plate. 'Arching' action is occurred through the concrete partial encasement, which is resisted by the end plate connections.

The common range of application for USFBs based is for slab depths of 180 to 300mm, in which the concrete is placed flush with top flange. The nature of the choice of UC for the bottom tee-sections and UB for the top tee-sections is that the asymmetry in flange areas can be over 3 to 1. Composite action reduces this effective asymmetry and improves the bending resistance. In practice, the span to depth ratio of USFBs is generally in the range of 25 to 30, which means that serviceability rather than bending or shear resistance will control [10]. Therefore, a further initial study has been conducted by the authors on the derivation of dynamic properties of USFBs through FE modal analysis and experimental verification [11].

### 3. Aim and objectives

The aim of this study is to investigate the contribution of concrete in perforated steel beams in resisting the vertical shear when the concrete is cast between the flanges of the steel beam. It should be noted that this experimental programme was intended to simulate a symmetric UB section without any mechanical shear connectors. The percentage of the section enhancement and its additional shear capacity when the web openings are in-filled with pure concrete was obtained. Consequently, the effect of the bond strength of the interface between the steel and the concrete, as well as the bearing strength of the open web area and the Vierendeel failure mechanism due to the confined concrete was explored in this research programme.

The main task was to validate the new approach and develop an elaborate model so it could be used for further studies such as vibration, dynamic analysis, etc. Hence, the sub-objectives of this research study are listed as follows:

- To demonstrate significant shear enhancement due to the concrete infill.
- To provide a minimum concrete vertical shear contribution that can be applied in all cases of USFBs based on the concrete encasement and the contact behaviour between the steel and the concrete.
- To establish FE models which are capable of predicting the structural behaviour of simply supported USFBs with large isolated circular web openings.
- To examine both the load carrying capacities and the failure modes of the USFBs. Also, to study the steel buckling behaviour, the concrete internal stresses (cracks), as well as the angles of the concrete cracks, both experimentally and through the FE analyses.
- To perform a sensitivity FE study based on both concrete and steel material properties and their constitutive relationships.
- To propose a simple design method of predicting the load carrying capacity of the particular steel-concrete beam arrangement.

### 4. Experimental work

Four USFBs were tested in this research programme. These are directly comparable with other experimental work conducted by the authors [12, 13]. Correspondingly, the web opening diameter,  $d_o$ , is equal to  $0.76h$ . For small web opening diameters, for instance 30% of the beams depth, it is easy to show that a load path of  $45^\circ$  between flanges transfer the load across the web opening. However, for larger web openings the load path is not so clear.

#### *4.1 Test specimen and measurement devices*

A UB305x165x40 with material physical properties shown in **Table 1** was used. For precautionary reasons it was decided to test all the beams at the 14<sup>th</sup> day of curing, aiming for between 25 to 30MPa (to be no greater than 35MPa) concrete strength on the day of the test.

The load was applied through two hydraulic jacks and a spreader plate. The applied load and hence the bending moments were obtained from the load cells connected to the jacks. High shear forces were generated in the area of the web openings and so the existence of the concrete dramatically affected the results.

To measure vertical deflection three dial gauges were placed under the tension steel flange and aligned with the edge of the hole. Two dial gauges were applied at the high moment side (HMS) of each web opening (Dial Gauge 1 and 3) and one dial gauge at mid-span of the test beams (Dial Gauge 2).

#### *4.2 Test cubes procedure*

In this research programme a desirable maximum compressive strength was required to determine the possible section enhancement at low concrete strengths. The strength was determined from the 14<sup>th</sup> day of curing to try and test at the minimum possible compressive strength used by the standards (i.e. 25MPa).

A mix design was necessary for this experimental programme. Compression tests were undertaken on samples, removed from the forms and allowed to cure for predetermined periods such as 3, 7, 14 days etc.. The concrete strength tests are standardized and the method of making compressive specimens in the field is covered under BS EN197:Part 1:2000 [14]. Based on the guidelines of BRE [15], the fourteen days compressive strength is equal to 85% of the twenty-eight days compressive strength. Moreover, thirteen days of air-cured concrete compressive strength is equal to 70% of the thirteen days water-cured concrete compressive strength. The mix with the  $w/c$  ratio equal to 0.61 conformed to the requirements and this was used for casting the composite beams.

#### *4.3 Casting the USFBs*

Four composite specimens were cast using Lafarge Blue Circle OPC CEM-I 42.5 N conforming to BS EN 197: Part 1 [14]. Sharp sand with a maximum size of 5mm was used as the fine aggregate. River gravel with a maximum size of 10mm was used as the coarse aggregate to overcome the problems associated with having to cast the specimen on one side (**Fig. 2**). Twenty-four hours ( $\pm 4$  hours) later, the specimens were de-moulded and left to air-cure in a storage room covered in sheeting for thirteen days. The storage room's temperature was 19 to 23°C at 50% to 60% relative humidity.

The casting of the composite beams was not routine because the bearing plates at the supports and the web openings make the whole procedure more difficult. This was accomplished by casting the beams on the floor and pouring the concrete through the web openings (**Fig. 2**). Vibrators were used to ensure that the concrete was well compacted. The compaction of the concrete was also improved by the high water-cement ratio (0.61). Silicon was used to avoid water leakage between the steel and the framework.

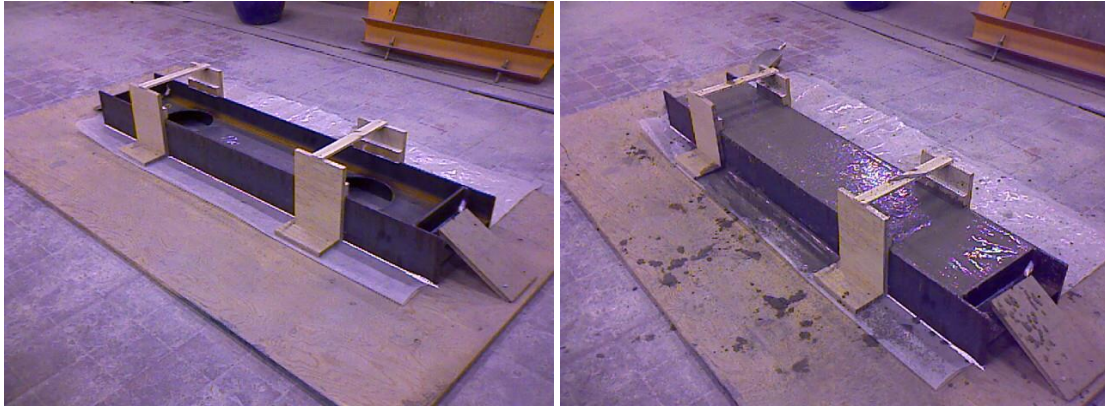


**Fig. 2:** Casting procedure of USFBs (i.e. USFB No. 1)

#### *4.4 USFB with lower grade concrete*

Three USFBs were cast with a  $w/c$  ratio equal to 0.61. Taking into consideration the usual uncertainties caused by human or climate interferences which occur when the beams are cast in situ, another composite section (USFB 4) was also cast with a slightly higher  $w/c$  ratio (and hence lower grade concrete). Segregation was observed when the concrete cubes of the latter specimen were tested. An additional aim of this test was to verify the percentage of the shear improvement and the failure mode due to concrete infill (i.e. concrete is a path to the load), and to clarify whether it is the concrete strength or the concrete itself that provides the enhancement to the perforated steel beam.

The compressive cube strength are shown in **Fig. 3**. USFB No.4 (i.e. Mix7) was tested after 52 days of curing as it needed more time to gain the required concrete strength limit (25-30MPa).

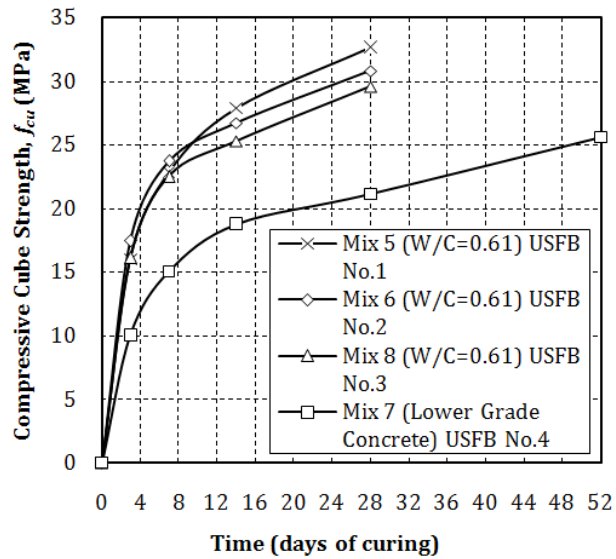


**Fig. 3:** Concrete cube compressive strength

Specimen	Average Steel Yield Stress $f_y$ (MPa)	Average Steel Tensile Strength $f_{ult}$ (MPa)	14-Day Cube Compressive Strength of Concrete, $f_{cu}$ (MPa)
USFB No.1			27.91
USFB No.2	318.25	430.75	26.77
USFB No.3			25.33
USFB No.4			25.60 (at 52 <sup>nd</sup> Day)

**Table 1:** Material physical properties

#### 4.5 Test procedure

After a preloading stage, the load was applied in steps at a low displacement rate and held at each step to allow load relaxation. All test specimens were loaded past the ultimate load to obtain a significant part of the post-failure curve. Concrete crack patterns were recorded throughout the tests.

Initially, the beams were loaded with approximately 10kN and the dial gauges zeroed. The load was then released and reloaded gradually in 40 to 50kN increments. The loading increments were reduced after the first diagonal cracking to approximately 20 to 30kN, up to the point of the beams' ultimate load carrying capacity. In the post-elastic region there was a further reduction to approximately 5 to 10kN per step. The tests were performed not only until the maximum load was reached, but also until a sufficient branch of the descending post-failure load deformation curve was recorded. The general test-procedure is summarised in the following four steps: i) preloading, ii) monotonic loading, iii) gradual loading and relaxation and iv) unloading.

#### 4.6 Load-deflection relationships

Virtually linear behaviour was observed in all tests (**Fig. 4**) until around 500kN which is at approximately 89% of the ultimate load carrying capacity of the composite beams. The ultimate load was attained at around 600kN, after which unloading occurred. Failure occurred around 75%, 67%, 70% and 71% of the maximum load for USFB No.1, USFB No.2, USFB No.3 and USFB No.4, respectively. Generally, in the post-elastic region a significant and sudden drop of load occurred directly after reaching the ultimate load capacity. This is a result of large concrete cracks occurring in the vicinity of the web openings and their rapid propagation, due to the steel yielding. The deflections were found to be higher in USFB No.1, where the post-elastic behaviour is more gradual than the other tests. Finally, an unloading procedure was conducted in all composite tests in order to record the plastic-permanent deformation. It should be noted that all USFBs have the same steel section stiffness. A dissimilar proportion of cracks about the symmetry of the beam was observed, with few cracks forming on one side as compared to the other side which was totally crushed. Similarly, in the bare steel perforated beam asymmetrical behaviour was observed between the left and right side.

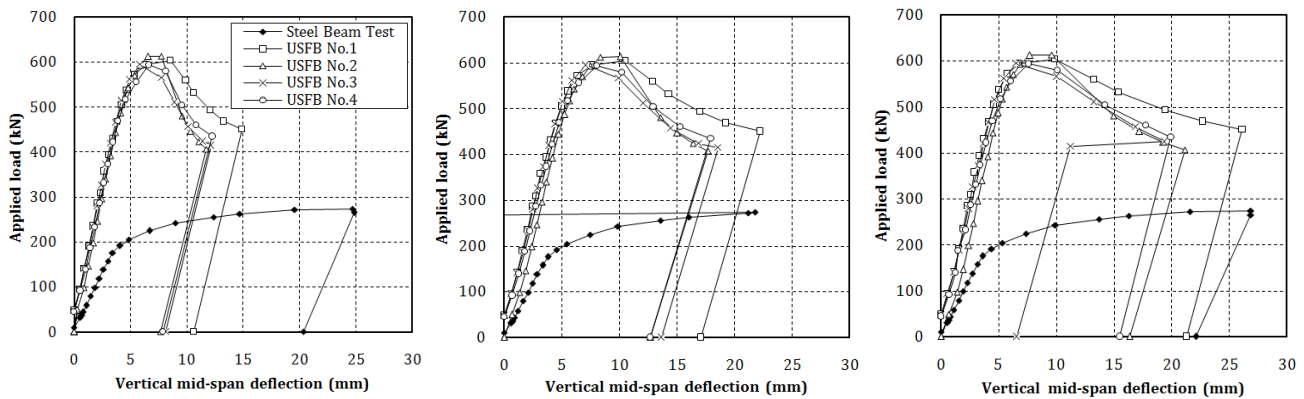


**Fig. 4:** Load-deflection curves for non-composite and composite beams for (Dial Gauge 1, 2 and 3)

#### 4.7 Failure mechanism

Diagonal tension cracks occurred at around 200 to 250kN. At about 300kN cracks could be clearly seen. The latter cracks were fully extended between the load spreader and the supports (e.g. **Fig. 5** and **6**). Also, at this point a few vertical flexural cracks were propagated in the region of maximum moments, starting from the tension face and extending upwards to the mid-depth of the beams. It is worth noting that this load was the ultimate load carrying capacity of the bare steel beam. At around 550kN the plasticity of the USFBs commenced. Full development of diagonal cracks ensued at this point in all composite beams. Eventually, crushing of the concrete occurred in the vicinity of the web openings as it is shown in **Fig. 7** and **8**. From the first load steps and during testing, micro-cracking was heard, especially for the USFB No.4 with the lower grade concrete, as the chemical bond of the concrete material was low (high  $w/c$  ratio). The

position of the principle diagonal cracks was not identical for all the USFBs. There is a slight variation of the angle of the cracks from  $25^\circ$  to  $37^\circ$ ; however the failure mechanism was the same. Around 600kN the ultimate load carrying capacity was achieved followed by a post-elastic descending curve showing a considerable decrease of the load carrying capacity. This was accompanied by large cracks in the vicinity of the web openings and concrete bursting. This can be seen in **Fig. 9** to **12** for the right half span of the USFBs, for both front and back face. Following the formation of the large cracks there was some residual strength in the concrete and the load carrying capacity was somewhat higher than that of the non-composite steel beam.

Essentially, USFBs fail due to concrete crushing in the compression zone. Complete composite action up to the ultimate load carrying capacity, was found. Therefore, the proposed system enables the development of sufficient strength and consequently effective composite behaviour, without causing serviceability problems. Moreover, the longitudinal shear strength of the proposed system consists of the frictional force and the shear-bond strength between the steel and the concrete, as well as of the bearing strength of the web opening area. However, in this experimental study the concrete is partially encased since the bearing plates at the supports restrain the longitudinal movement of the concrete. In actual construction the end plate connections will play the same role. Also, it was observed that the plastic behaviour of the composite sections is mainly due to the steel beam's low stiffness and high deformation. In general, the concrete provides a load path from the top to the bottom steel flange, as well as a restraint to the steel web.

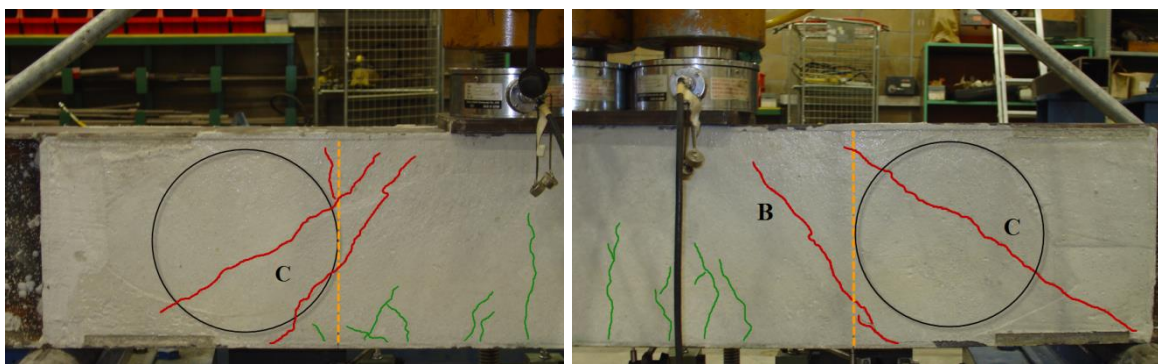


**Fig. 5:** USFB No.2



**Fig. 6:** USFB No.3



**Fig. 7:** USFB No.2 at point D with concrete crushing



**Fig. 8:** USFB No.3 at point D with concrete crushing



**Fig. 9:** USFB No.1 with concrete bursting

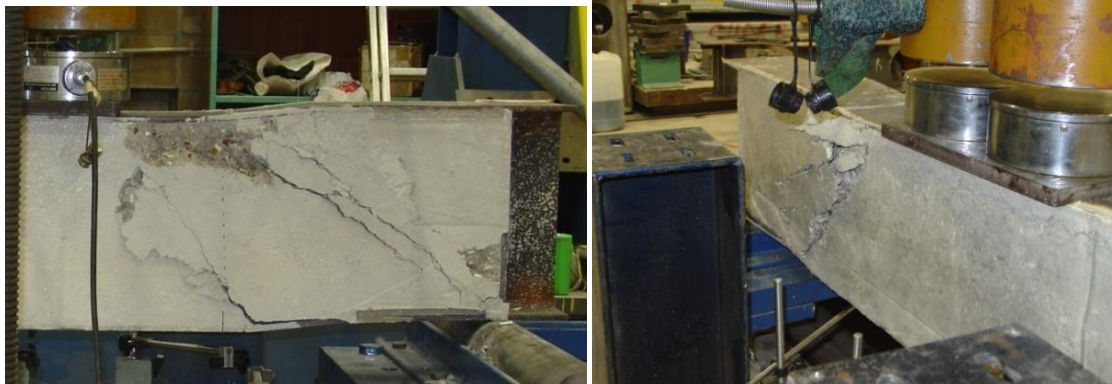


**Fig. 10:** USFB No.2 with concrete bursting



**Fig. 11:** USFB No.3 with concrete bursting



**Fig. 12:** USFB No.4 with concrete bursting

#### *4.8 Composite action due to partial encasement*

The effect of partial encasement on overall flexural action is dependent on the mechanism of shear transfer and the relative slip between the steel section and the concrete. These tests failed by high Vierendeel bending actions in the vicinity of the openings, as shown in **Fig. 13** and **14**. However, it is apparent that considerable 'arching' action occurred through the concrete encasement, which is resisted by the bearing plates at the supports of the relatively short span beams. Hence, the contribution of the confined concrete between the steel flanges in resisting vertical shear is achieved.

Following the completion of the composite tests the crushed concrete was removed from the area around the web openings. It is worth mentioning that the concrete was removed only by using a hammer and manpower - no heavy equipment was used in trying to remove the crushed concrete. This helps to visualize the size of the concrete area around the web opening that is strongly affected by the web opening existence.

The steel beam was slightly deformed compared to the non-composite beam [12], while local web buckling is faintly observed on the diagonal line from the load spreader to the supports. This implies a transfer of shear forces across the web openings after the concrete crushed while loading was applied in the post-elastic region. The transfer of shear forces caused local bending moments and therefore local web buckling.

At the web opening the concrete encasement acts as a strut in compression, which is confined between the flanges and inclined diagonally across the web opening, as illustrated in **Fig. 15**. The magnitude of this strut action depends on the ability of the flanges to resist the local compression forces by transverse bending. The dimensions of the flanges contribute significantly to the bending and shear resistances of USFBs [16, 17]. It is worth noting that a symmetric section was used in the current research to simplify the investigation, whilst asymmetric sections are used in practice. The transverse bending moment is shown in **Fig. 16** when the bearing force applies on the flange. The vertical forces are resisted by tension in the web-post between the web openings. The horizontal forces act on the bottom flange with a combination of friction, due to the strut force and the shear-bond. The lower bound of the shear-bond strength with the partially encased flange is given as 0.2MPa in BS EN1994-1-1:2004 [18]. A coefficient of friction of 0.6 for concrete on steel may be assumed for the local strut action.



**Fig. 13:** Failure mode for partially encased USFB No.1 at opening after removal of the damaged concrete



**Fig. 14:** Failure mode for partially encased USFB No.2 at opening after removal of the damaged concrete

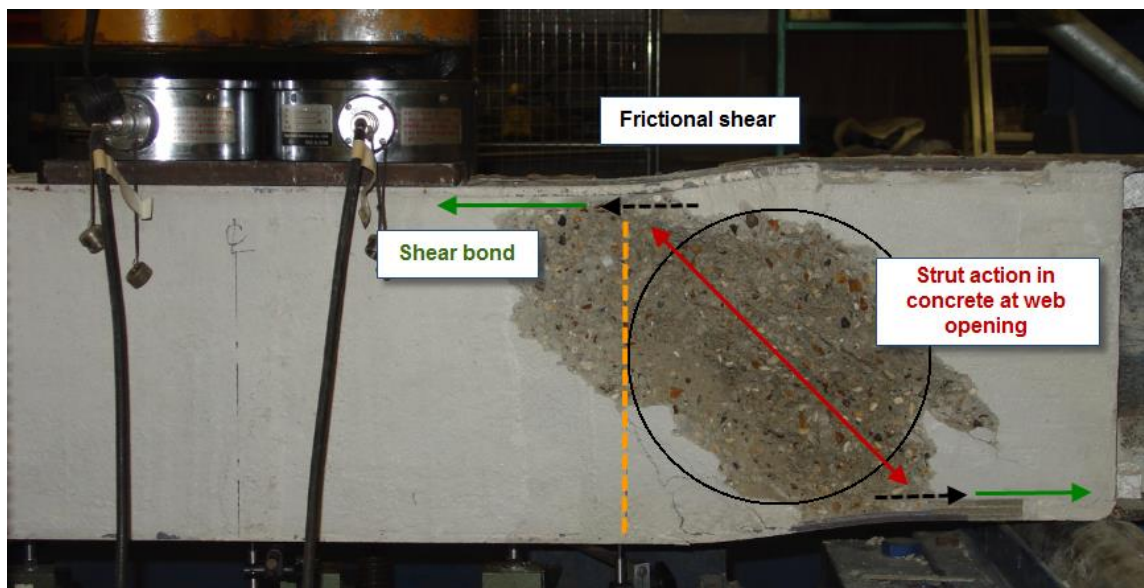


**Fig. 15:** Compression force acting in the concrete encasement across the web openings

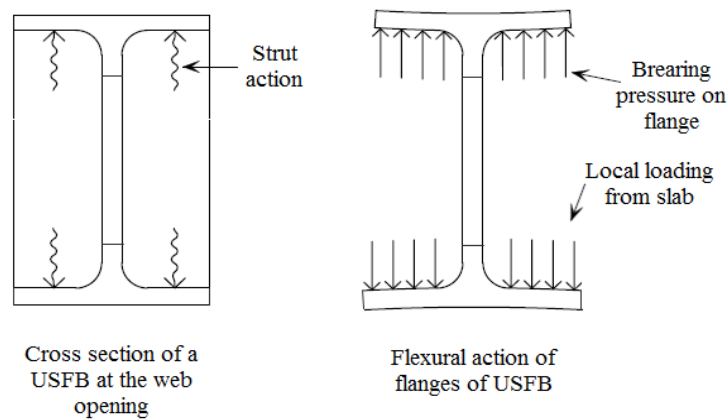


**Fig. 16:** Strut action in concrete causing flexural bending

A simple model for the vertical shear resistance of the concrete encasement is to consider the vertical component of this strut force as a bearing force which causes transverse bending in the flanges. From the above tests as well as others conducted at City University London [19], it was concluded that the shear force,  $V_c$ , that is resisted by the concrete encasement is dependent on the top flange dimensions and may be taken as [10]:

$$V_c = \frac{0.83 \left( \frac{d_o}{b_{f,min}} \right) t_f^2 f_y}{\cos \theta} \leq 0.2 b_{f,min} d_o f_{cu} \quad (1)$$

Where  $b_{f,min}$  is the lesser thickness of the top and bottom flanges. In using this formula, the ability of the flanges to resist the horizontal component of the force is dependent on the frictional force and shear-bond resistance, which is not critical, given the inclination  $\theta$  of the strut force to the vertical, where:

$$\theta = \tan^{-1}(0.5d_o/h) \quad (2)$$

The compression resistance of the concrete strut may govern for thick steel flanges. It is given by the limit in the above equation, and it may govern when  $b_f/t_f < 7$ .

## 5. Sensitivity FE study of the USFBs

### 5.1 Introduction

For the computational approach to the problem, a three-dimensional FE model was developed, in which contact elements were implemented at the interface of the concrete and steel. Several material model parameters were varied, such as the steel and concrete strength, the constitutive relationships which model the materials, as well as the steel and concrete contact capacity. Hence, the parameters that limit the beams' load carrying capacity and their sensitivity to these changes are examined.

A FE model was developed in ANSYS v11.0 to further investigate the load-deflection behaviour and failure modes of the composite USFBs. Due to the introduction of concrete in the FE models a complex non-linear analysis was developed. Consequently, a detailed description of the techniques and tools used to apply the boundary conditions and the material properties was also made. Apart from the geometrical and material non-linearity, the contact surface between the steel and the concrete takes a decisive role in modelling the friction between these two materials when no mechanical connectors are provided. The characteristics of the contact elements were determined individually by shear-bond tests (i.e. push-out tests) between the steel and concrete, conducted at City University London's laboratories [19].

## 5.2 FE model and boundary conditions

Since a principal objective of this work was to predict a correct failure mode, it was important to develop a FE model as close to the physical system as possible (**Fig. 19**). Therefore, a 3D model was developed with a fine mesh of 20mm element size consisting of 68,569 elements. With regards to the concrete crack modelling with FE software, several researchers have studied the effect of the element size in the non-linear analysis of reinforced concrete structures [20, 21], and they have shown that the results are indeed dependent on the mesh. Whilst considering symmetry, it was decided to develop the full model in terms of its length and the half model in terms of its width, in order to accurately apply the support conditions. The load and the supports were directly applied to the steel beam and not to the concrete in order to avoid early local concrete cracking. For better stress distribution, the load was applied as a pressure on an area and the supports were modelled as restrictions to the degrees of freedom on appropriate areas.

## 5.3 Contact element and contact algorithm

CONTA173 is a 4-node element that is intended for flexible-to-flexible contact analysis. In flexible-to-flexible contact, both contact and target surfaces are associated with deformable bodies. CONTA173 is also a surface-to-surface contact element. The contact detection points are the integration points and are located at Gauss points. The contact elements are constrained against penetration into the target surface, at its integration points.

A number of methods are available for modelling friction in contact analyses, but the most commonly used methods are based on a 'Coulomb' friction model. In this model the two contacting surfaces are permitted to carry shear stresses across their interface up to a defined value, before they begin sliding. The equivalent shear stress at which sliding begins is defined as:

$$\tau_{slide} = \mu P_{Con} + CSR \quad (3)$$

Contact elements offer two models for 'Coulomb' friction: isotropic friction and orthotropic friction. The isotropic friction model is incorporated in this study as it uses a single coefficient of friction, based on the assumption of uniform stick-slip behaviour in all directions. When a penetrating node stays in contact with the target surface, it may either stick to the surface or slip along the surface.

## 5.4 Element types and material models

Steel: Typical 8-node solid SOLID45 elements were used to model the steel perforated beam. Mainly nominal, but also actual measured, material properties were used. This was for precautionary reasons, as well as for the generalization of the FE results. The bi-linear stress-strain relationship for both compression and tension with strain hardening used, show sufficient agreement with the previous

experimental study of the non-composite steel beam [12, 13, 22, 23]. The Young's Modulus,  $E$ , and the Poisson's Ratio,  $\nu$ , of steel are taken as 205GPa and 0.3 respectively. The yield strength,  $f_y$ , as well as the ultimate strength,  $f_{ult}$ , varies as given in **Table 3**. The variation of the material strength applies to the sensitivity study of the material properties. In most analyses, an ultimate strain of around 0.25 was assumed for the structural steel [24], hence the Tangent Modulus,  $E_T$ , was varied from 540 to 700MPa.

Concrete: 8-node solid iso-parametric SOLID65 elements with the integration points for the cracking and crushing checks were used to model the concrete in ANSYS. SOLID65 models the non-linear response of brittle materials and is based on a constitutive model for the tri-axial behaviour of concrete after Williams and Warnke [25]. The element is capable of plastic deformation and cracking in three orthogonal directions. Once the principal stresses at the integration points reach the tensile and compressive strength, the cracking or crushing of concrete elements can be formed. These elements are also able to predict the non-linear behaviour of concrete materials using a smeared approach, which depends on five material parameters. Steel reinforcement was not present in the actual experiment in this research programme; hence default values were kept for the smeared reinforcement capabilities of SOLID54 elements.

Cracking and crushing are determined by a failure surface. The tensile strength,  $f_t$ , is typically 8-15% of the compressive strength,  $f_c$  [26]. Investigating the sensitivity of the results, the ultimate concrete compressive and tensile strengths for every beam model were calculated using various constitutive relationships found in the literature [25, 27, 28, 29, 30]. The concrete in compression was modelled as an elasto-plastic material (**Fig. 17**) either with or without strain softening. The concrete plasticity (crushing) in the compression zone was modelled using the multi-linear option from ANSYS with Von-Mises plasticity.

The compressive cylinder strength,  $f_c$ , varied (eg. 20MPa, 21.12MPa: the average cylinder strength from **Table 1**, 26.7MPa and 32MPa), whereas the other parameters such as Young's Modulus,  $E_c$ , and tensile strength of concrete,  $f_t$ , are treated as generic data and evaluated by the applying constitutive relationships (**Table 2**). In **Table 2**,  $f_c$  is the stress at any strain  $\varepsilon$ ,  $f_1$  is the stress at strain  $\varepsilon_1$  and  $\varepsilon_o$  is the strain at the ultimate concrete cylinder compressive strength  $f_c$  ( $f_c = 0.8f_{cu}$  was always used).

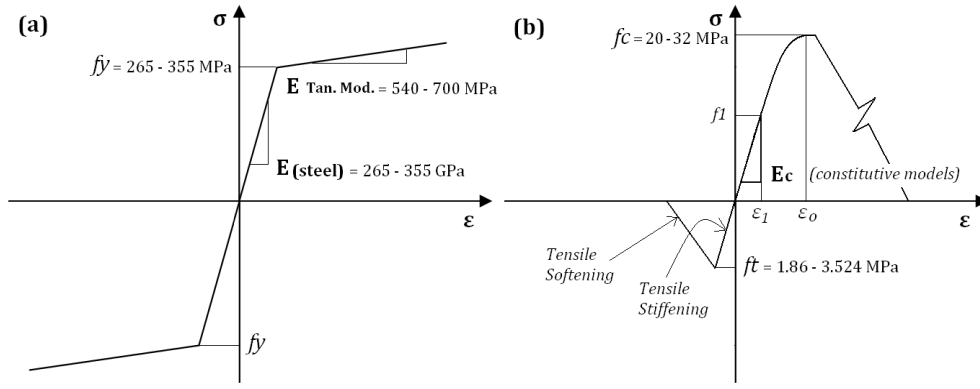


**Fig. 17:** Material models of uni-axial loading: (a) Steel and (b) concrete

Reference (in SI)	$E_c$	$f_t$ and $\varepsilon_o$	$f_1$ and $\varepsilon_1$	$f_c$	$\beta$ coefficient
[25]	$E_c = 5050\sqrt{f_c}$	$f_t = 0.545\sqrt{f_c}$	$f_1 = 0.4f_c$ (HSC)	$f_c = \frac{\beta \left(\frac{\varepsilon}{\varepsilon_o}\right) f_c}{\beta - 1 + \left(\frac{\varepsilon}{\varepsilon_o}\right)^\beta}$	$\beta = \left(\frac{f_c}{32.4}\right)^3 + 1.55$
	$\nu = 0.15$	$\varepsilon_o = 0.002$	$\varepsilon_1 = \frac{f_1}{E_c}$		
[27] Standards: ACI318-99 [30]	$E_c = 4730\sqrt{f_c}$	$f_t = 0.623\sqrt{f_c}$	$f_1 = 0.3f_c$	$f_c = \frac{E_c \varepsilon}{1 + \left(\frac{\varepsilon}{\varepsilon_o}\right)^2}$	---
	$\nu = 0.2$	$\varepsilon_o = \frac{2f_c}{E_c}$	$\varepsilon_1 = \frac{f_1}{E_c}$		
[28] Standards: AS3600-09 [31]	$E_c = 5050\sqrt{f_c}$	$f_t = 0.4\sqrt{f_c}$	N.A.	$f_c = \frac{E_c \varepsilon}{1 + \left(\frac{\varepsilon}{\varepsilon_o}\right)^2}$	---
	$\nu = 0.3$	$\varepsilon_o = \frac{2p_c}{E_c}$ (apprx. 0.2% proof stress)	$\varepsilon_1 = \frac{f_1}{E_c}$		
[29] Standards: BS 8110-97 [32]	$E_c = 9100(f_c)^{1/3}$	$f_t = 0.36\sqrt{f_c}$	N.A.	$f_c = \frac{E_c \varepsilon}{1 + \left(\frac{\varepsilon}{\varepsilon_o}\right)^2}$	---
	$\nu = 0.2$	$\varepsilon_o = \frac{2f_c}{E_c}$	$\varepsilon_1 = \frac{f_1}{E_c}$		

**Table 2:** Constitutive relationships modelling the concrete material from the literature

Concrete compressive strength was varied in order to examine the percentage of shear enhancement of the USFBs. The concrete tensile strength was also varied taking into consideration the mesh size of the concrete elements and the value of fracture energy,  $G_f$ . It is worth noting that the interfacial fracture energy is almost linearly related to the root of the tensile strength of concrete. In addition, various values of concrete Poisson's ratio,  $\nu$ , were examined, as they are related to the condition (i.e. quality) of concrete and different values have been used by researchers.

Shear Transfer Coefficient for open/closed crack,  $\beta_{1,2}$ : These are also known as "shear retention factors" and can vary between '0.0' for no aggregate interlock and 1.0 for full aggregate interlock. In the opening,  $\beta_1$  or closing  $\beta_2$  are assumed to take a value of 0.25 and 0.7 respectively for plain concrete of all grades.

Various shear transfer coefficients are used in this study for open cracks and closed cracks. High values were taken for the closed crack (e.g. 0.9, 1.0) so as to prevent possible fictitious crushing of the concrete before load transfer occurs through a closed crack.

Friction Coefficient,  $\mu$ : Various friction coefficients were used in order to compare the results. The results showed an increase of the stiffness in the strain of the compressive top flange for beam with higher bond, but in the tensile flange the stiffness is nearly the same. A reason for this behaviour is the cracking of concrete in tensile zone, which starts from the first load steps. In the experiments the bond strength is also different in the compressive zone from that in the tensile zone of the composite beam, and this could be another reason for possible discrepancy between the experimental and the FE results. The local bond strength and the corresponding slip are almost linearly related to the tensile strength of concrete.

Solution Method: The full Newton-Raphson procedure was used, even though this requires the stiffness of the structure to be re-calculated for every iteration. A large-displacement and static analysis was implemented with the maximum number of sub-steps in a load step being 1,000-10,000 in order to apply the load increments very smoothly where it is necessary. Failure of the beam occurs when convergence fails, with a very small load increment. This method is comparable with the experimental data from Buckhouse [33]. The vertical deflection at mid-span of the composite beams and the FE divergence load was monitored.

### *5.5 FE results from sensitivity study*

The failure loads obtained from this study are summarised in **Table 3** and categorised mainly according to the constitutive relationships used to model the material properties. Sub-categories are also indicated, based on both the steel and concrete strengths.

It was observed that the numerical solutions are very sensitive to the steel strength in contrast to the concrete strength and small changes lead to significantly different results. It is found that the USFBs with steel yield strength of 265 to 285MPa compare well with the experimental behaviour, even though there is a reduction of 16.8 to 10.5% in the average steel yield strength (i.e.  $f_y=318.25MPa$ ), as obtained from the coupon tests. This applies to the increased stiffness of the 3D solid elements as well as the complex failure mechanism of the USFBs. Essentially, it was verified that the ultimate load carrying capacity of the USFBs is governed by the steel strength and in particular when the concrete strength is low.

Furthermore, it is apparent that apart from the steel and concrete strength, the shear transfer coefficients and the coefficient of friction play a significant role in simulating the structural behaviour. It was found that the most effective applicable factors for opened and closed cracks,  $\beta_1$  and  $\beta_2$ , are 0.3 and 1.0,

respectively. Dramatic change of the divergence load is obtained when the coefficient of friction,  $\mu$ , is reduced significantly (eg.  $\mu=0.4$ ). For  $\mu$  greater than 0.6 full cracks were recorded. Similarly, full cracks were recorded when the yield strength of the steel is greater than 300MPa. The discrepancy for the value of ultimate load obtained by means of the numerical solution and experiment was about 22.5% using solid elements, while it was only 4.5% using shell elements. Observing the real tests it was found that no slip occurred between the steel and the concrete up to the yield point. Subsequently, a value of 1.0 (i.e. perfect bonding) was mainly used at the contact surface. For  $\mu \neq 1.0$ , a significant interlocking between the steel and the concrete exists after de-bonding due to the non-uniform strain across the section of the member.

\*MISO – Multi-linear Isotropic Hardening Plasticity is adopted

\*\*BISO – Bi-linear Isotropic Hardening Plasticity is adopted

Steel		Cont.	Concrete					Results	FE Model
$f_y$ (MPa)	$f_{ult.}$ (MPa) or $E_{Tan.}$	$\mu$	$f_c$ (MPa)	$f_t$ (MPa)	$\nu$	$\beta_{1,2}$	Refer. Theory Based	$F_{FEA}$ (kN)	
265*	410	1.0	26.70	1.86	0.20	0.3,1.0	[28]	<b>627</b>	59
265*	410	1.0	26.70	1.86	0.17	0.3,1.0	[28]	<b>617</b>	3
265*	410	0.8	26.70	1.86	0.17	0.3,1.0	[28]	<b>611</b>	7
265*	410	0.3	26.70	1.86	0.17	0.3,1.0	[28]	<b>548</b>	8
265*	410	1.0	26.70	1.86	0.15	0.3,1.0	[28]	<b>547</b>	58
265*	410	1.0	26.70	1.86	0.15	0.6,0.6	[28]	<b>555</b>	16
265*	410	1.0	26.70	1.86	0.15	0.1,0.9	[28]	<b>607</b>	18
265*	410	1.0	26.70	1.86	0.15	1.0,1.0	[28]	<b>635</b>	19
265*	410	1.0	26.70	1.86	0.00	1.0,1.0	[28]	<b>648</b>	20
275**	$E_{Tan.}=200$	0.8	26.70	1.86	0.15	0.1,0.9	[28]	<b>618</b>	25
355*	530	1.0	26.70	1.86	0.20	0.3,1.0	[28]	<b>637</b>	11
355*	530	1.0	26.70	1.86	0.17	0.3,1.0	[28]	<b>633</b>	12
355*	530	0.0	26.70	1.86	0.17	0.3,1.0	[28]	<b>470</b>	13
275*	410	0.9	20.00	2.786	0.2	0.3,1.0	[26]	<b>577</b>	B5
275*	410	0.6	20.00	2.786	0.2	0.3,1.0	[26]	<b>563</b>	B6
355*	499	0.9	20.00	2.786	0.2	0.3,1.0	[26]	<b>730</b>	B2
355*	530	0.9	20.00	2.786	0.2	0.3,1.0	[26]	<b>733</b>	B4
355**	$E_{Tan.}=20$	0.9	20.00	2.786	0.2	0.3,1.0	[26]	<b>734</b>	B3
275*	410	1.0	21.12	2.863	0.2	0.3,1.0	[26]	<b>591</b>	B11
275*	410	0.9	21.12	2.863	0.2	0.3,1.0	[26]	<b>584</b>	B10
275*	410	0.7	21.12	2.863	0.2	0.3,1.0	[26]	<b>578</b>	B12
275*	410	0.4	21.12	2.863	0.2	0.3,1.0	[26]	<b>508</b>	C8
275*	410	1.0	21.12	2.863	0.2	1.0,1.0	[26]	<b>599</b>	B13
318.25*	430	1.0	21.12	2.863	0.2	0.3,1.0	[26]	<b>630</b>	D1
265*	410	0.9	32.00	3.524	0.2	0.3,1.0	[26]	<b>588</b>	C1
275*	410	0.9	32.00	3.524	0.2	0.3,1.0	[26]	<b>611</b>	C4
275*	410	0.6	32.00	3.524	0.2	0.3,1.0	[26]	<b>574</b>	C14
285**	$E_{Tan.}=20$	0.9	32.00	3.524	0.2	0.3,1.0	[26]	<b>622</b>	C6
285*	350	0.9	32.00	3.524	0.2	0.3,1.0	[26]	<b>641</b>	C5
355*	499	0.9	32.00	3.524	0.2	0.3,1.0	[26]	<b>742</b>	B1
275*	410	0.9	21.12	1.839	0.3	0.3,1.0	[27]	<b>545</b>	B9
275*	410	0.9	32.00	2.260	0.3	0.3,1.0	[27]	<b>621</b>	C12
275*	410	0.6	32.00	2.260	0.3	0.3,1.0	[27]	<b>597</b>	C13
275*	410	0.7	21.12	2.505	0.15	0.3,1.0	[24]	<b>571</b>	C11
265*	410	1.0	32.00	3.083	0.15	0.3,1.0	[24]	<b>629</b>	31
265*	410	0.8	32.00	3.083	0.15	0.3,1.0	[24]	<b>600</b>	32
265*	410	0.5	32.00	3.083	0.15	0.3,1.0	[24]	<b>565</b>	33
275*	410	0.9	32.00	3.083	0.15	0.3,1.0	[24]	<b>615</b>	B14
275*	410	0.9	32.00	3.083	0.15	0.0,1.0	[24]	<b>243</b>	B15
<b>BARE STEEL PERFORATED BEAM</b>									
265*	410	---	---	---	---	---	---	<b>331</b>	60
318.25**	430	---	---	---	---	---	---	<b>352</b>	75
355**	$E_{Tan.}=2000$	---	---	---	---	---	---	<b>352</b>	61

**Table 3:** Results of the FE parametric study

### 5.6 Load-deflection relationships

Various load-deflection curves at the mid-span are plotted against the results of the experimental test of USFB No.1 (**Fig. 18**). In addition, the load-deflection curve of the non-composite perforated beam is plotted for comparison.

Most of the FE results correlate satisfactorily with the experimental results, while up to the ultimate load level insignificant steel deflection occurs. Thereafter, the steel yields following the large concrete strains and the formation of large cracks, whilst the load capacity drops considerably. For the USFB with the lower concrete compressive strength more cracks developed even though the capacity of the USFB remained the same. In the experimental tests large steel deflections ensue in the post-elastic curve.

There are several effects that might cause the deviation of the stiffness between the FE and the experimental beams. One reason could be the concrete micro-cracks in the experimental beams due to drying shrinkage in the concrete. Additionally, cracks generated from different elastic modulus of aggregate and cement, thermal effects, as well as human factors could cause reduction of the stiffness in the experimental beams.

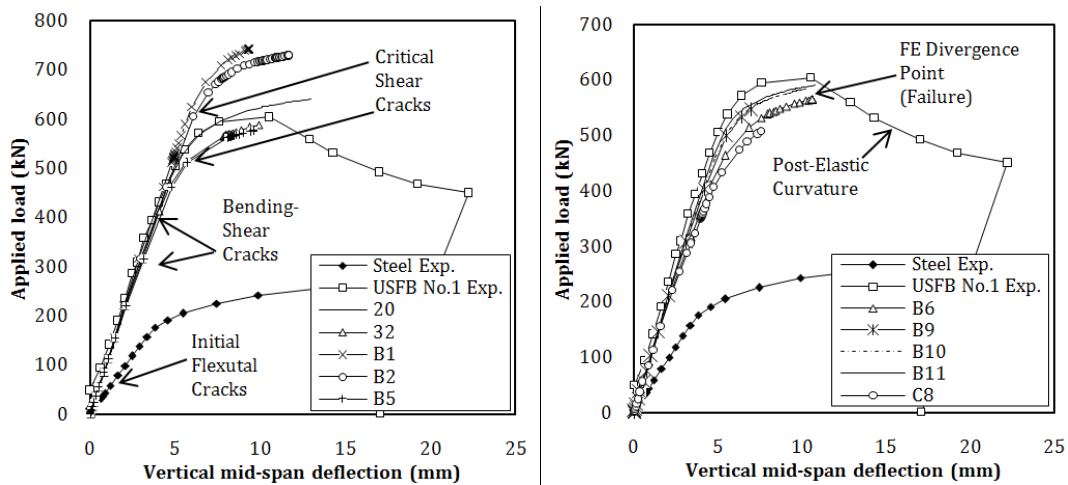


**Fig. 18:** Force-deflection curves comparison between experimental test (USFB No.1) and various numerical solutions from “Table 2”

### 5.7 Post-elastic behaviour in FEA

The maximum load is recorded following the divergence of the FE analysis. The problem of implicit solvers is the sudden loss of stiffness if the material failure is taken into account [34]. The last descending branch of the load-deflection curve corresponds to the composite beam behaviour as a ‘mechanism’. The load which the system can carry gradually decreases with increasing deflection, while at some point no more loads can be resisted and the beam ‘fails’. In the experimental work, the failure was accompanied by appearance of wide intensive diagonal concrete crushing. In the finite element analysis, post-peak

softening usually means a localisation of failure. Hence, some special techniques such as non-local mode, gradient or time dependent formulations (explicit solvers) need to be employed.

The Newton-Raphson method used in this research proved to be generally economical because much larger incremental steps were possible. However, in the regions of peak loads on the load-deflection response, numerical difficulties sometimes occurred and it is necessary to use the modified Newton-Raphson iteration scheme under which the stiffness of the structure is calculated only at the beginning of the increment, or the modified Riks (Arc-length) method in order to prevent local instabilities due to large amounts of cracking.

To trace a post-peak response, either a quasi-static (transient), a stabilisation solver usually with an energy dissipation factor, an arc-length method or a displacement load control is necessary. The most widely utilised is the arc-length method in ANSYS, which controls the load level together with the length of the displacement increment. This method permits to compute the post-critical load-deflection path.

#### *5.8 Concrete crack patterns and failure modes*

Thirty-nine numerical tests are presented simulating the particular USFB configuration using different constitutive relationships and parameters. It is worth noting that in all cases the flexural and the diagonal cracks were generated. Characteristic results of concrete cracks, slippage profiles and steel stresses at the contact surface between the steel and the concrete are plotted. By examining the stress distribution, it was seen that failure occurred due to substantial steel yielding, combined with concrete crushing.

In **Fig. 19** the crack development is shown for four load steps. Nonlinear numerical solutions are capable of replicating the full range of cracks including the pure flexural, flexural shear and the critical shear crack. Smeared cracks are spread over the high shear stress region (**Fig. 19 (c)**) and occur mostly at the ends of the beam between the support and loading area. The path of shear cracks follows the trajectory of the principal stresses, as can also be seen in the experimental study. Depending on the geometric as well as the material properties of the USFB, the critical crack might extend to the top of the compression concrete fibres and then stabilise, as shown in **Fig. 19 (d)**. At the ultimate load carrying capacity the vertical beam deflections were not large.

Analytically, diagonal shear failure begins with the development of a few vertical flexural cracks at the mid-span, followed by a break of the bond between the bottom steel flange and the concrete. A critical shear diagonal crack develops in the vicinity of the web openings of the steel perforated beam. Very small flexural cracks appear from the beginning of the test, while shear diagonal cracks are not developed until the load level of approximately 400kN. Similar behaviour was observed at around 250 to 300kN, when the experimental tests were conducted. By looking at the inside view of the FE model (**Fig. 20**), it was found

that the cracks begin at the mid-width of the beam section, where the concrete passes through the web openings and more specific cracks are initiated as the steel web starts to deflect. These cracks are fully developed in the vicinity of the web openings at approximately 450kN, while cracks move outwards (i.e. transverse to the web). Crack propagation and the steel stresses at the mid-width of a USFB are shown in **Fig. 20**.

The vertical deflection, contact stresses and the contact surface condition for the particular USFB FE model, when using a friction coefficient,  $\mu$ , equal to 0.9, are presented in **Fig. 21**. The Von-Mises stresses of the steel beam for the particular USFB model are also presented in **Fig. 21**.

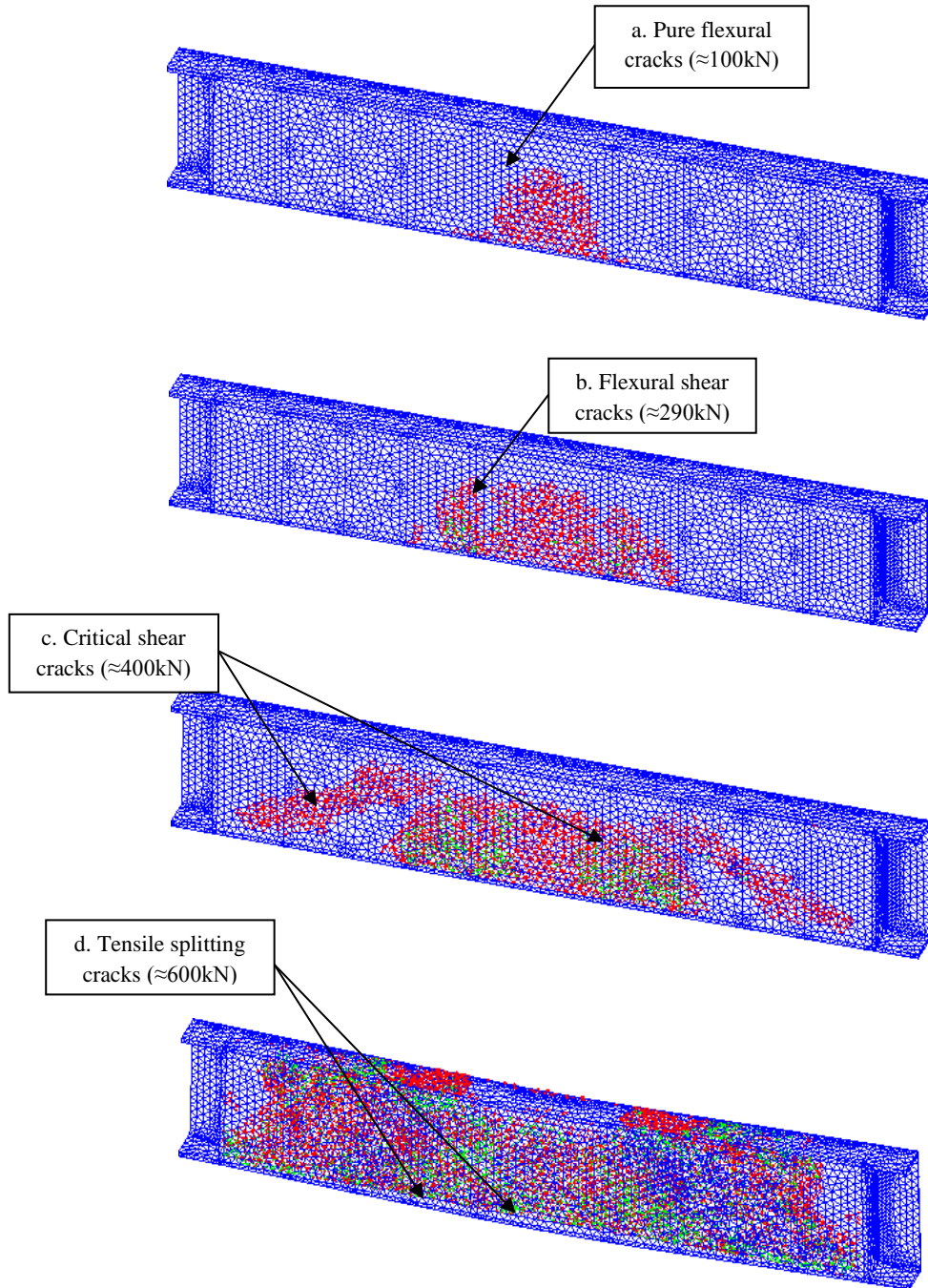


**Fig. 19:** Bending and shear crack development at the front side of the beam; (a) Purely flexural (bending) vertical cracks, no yielding in steel, no concrete plasticity (b) Developed flexural cracks, developed flexural/shear cracks, just before initiation of the critical shear cracks (c) Critical shear diagonal cracks are clearly identified and (d) Full cracking state, yielding in steel, concrete plasticity, big displacements increment just before divergence of the FE model, there are splitting cracks at the upper part of the beam due to compression

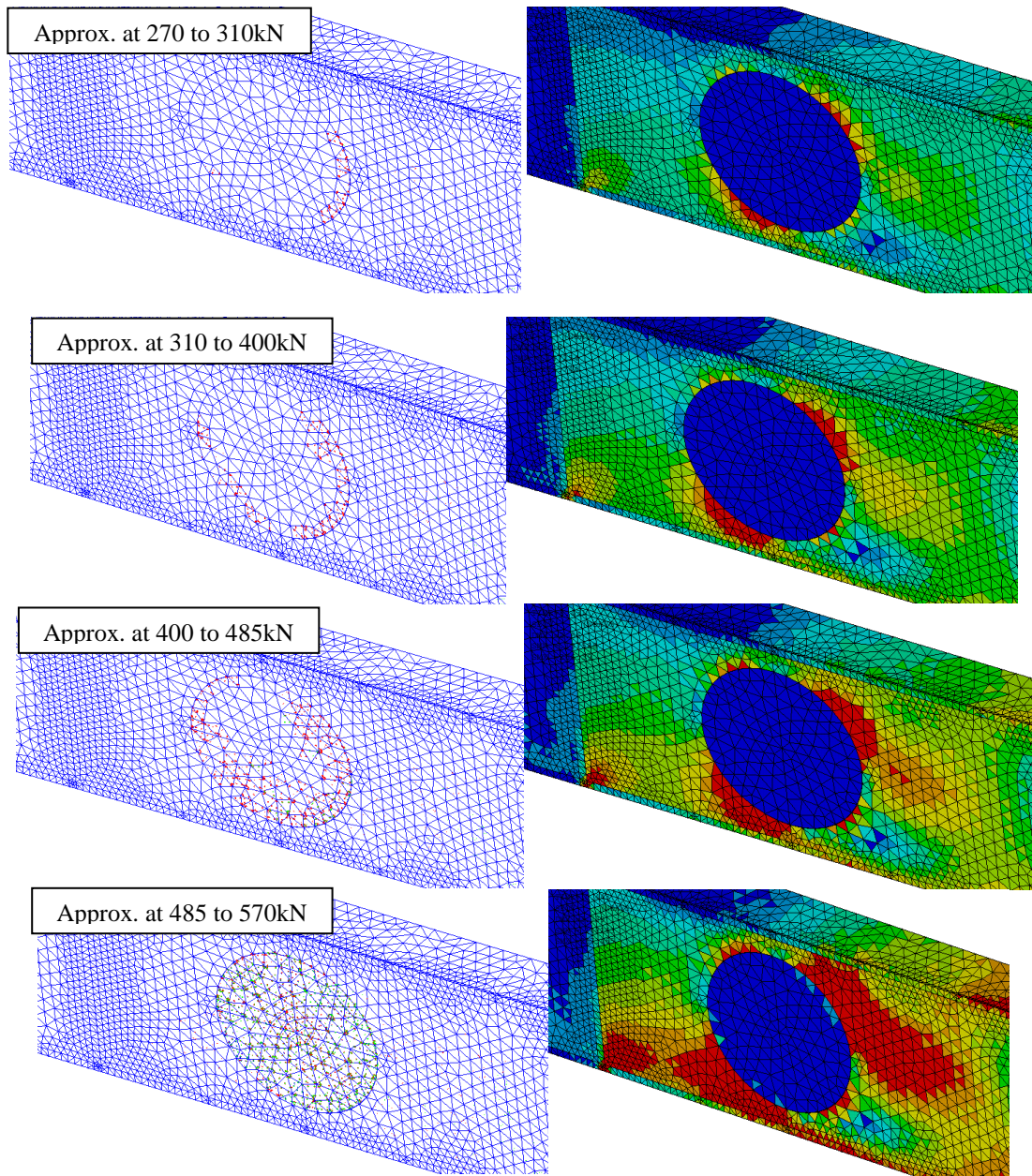


**Fig 20:** Shear crack development (left) and Von-Mises stresses of the steel (right); in the vicinity of the right web opening at the mid-width of a USFB

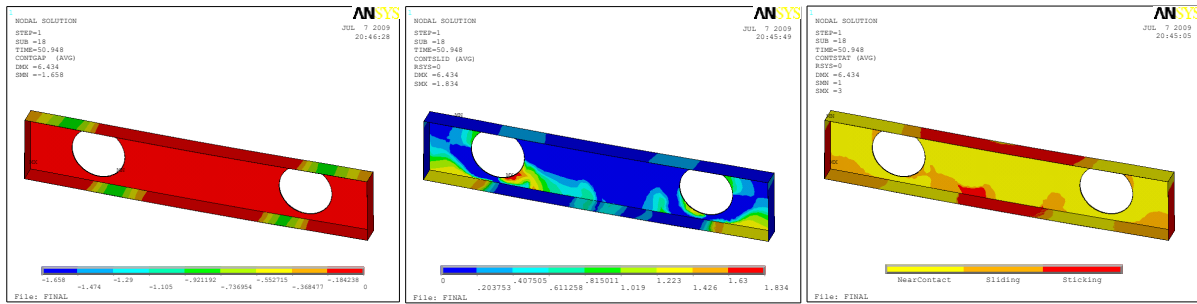


**Fig. 21:** Vertical deflection (left), contact stresses (middle) and contact surface condition (right)

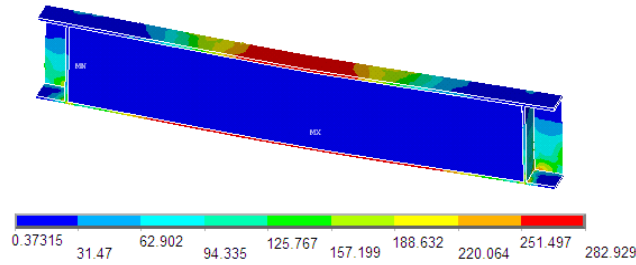


**Fig. 21:** Von-Mises stresses in the steel beam

## 6. Proposed design method evaluating vertical shear strength

The experimental programme and non-linear FE analyses showed that the concrete in-fill in the perforated sections and the composite action enhance the vertical shear strength of the USFB. Liang et al. [24] proposed a design method for the vertical shear strength of simply supported conventional unperforated composite beams (where the concrete slab sits on top of the plain steel beam) with any degree of shear connection. This method is modified herein to include USFB sections. Comparison is then made amongst the different approaches for evaluating the vertical shear strength of the perforated sections.

The composite action as presented by Liang et al. [24] is as follows:

$$V_{uo} = V_o(1 + 1.295\sqrt{\beta}) \quad (0 \leq \beta \leq 1) \quad (4)$$

When  $\beta > 1$ , the vertical shear strength is not affected by the degree of shear connection and this indicates that the composite beam exhibits full shear connection. According to BS5950 and EC3, for symmetric beams with spans up to 6m and 5m respectively, the minimum degree of shear connection is 0.4. In general, when no mechanical shear connection (i.e. reinforcement tie-bars, studs, ducting, etc.) is provided between the steel beam and the concrete slab, the two components work independently to resist vertical shear. However, in this particular FE study the degree of shear connection is assumed equal to the friction coefficient between the steel and the concrete, simulating the frictional force and shear-bond since no mechanical shear connection is provided.

Hence, the vertical shear strength of such a beam is expressed by:

$$V_o = V_c + V_s \quad (5)$$

The contribution of the concrete is now taken as the shear strength of the concrete infill and it is proposed that:

$$V_c = 1.16(f_c)^{1/3} A_{ec} \quad (6)$$

The effective shear area of concrete is evaluated as:

$$A_{ec} = (b_f - t_w)(h - 2t_f) - 0.86r^2 \quad (7)$$

It should be mentioned that the concrete in the web opening, as well as the effect of longitudinal steel reinforcement in the concrete slab, are not considered in the above equation.

In order to better correlate the theoretical approach with FE analyses and experiments, the shear capacity of the steel beam is evaluated with various approaches such as the following:

1. The basic shear capacity from Chung et al. [17]:

$$V_s = V_{o,Rd} = \frac{0.577f_y}{\gamma_{Mo}} \left[ (ht_w + 2(0.75t_f^2)) - d_o t_w \right] \quad (8)$$

2. Another approach for the shear resistance for perforated beams (Lawson and Hicks, 2006) is shown below:

$$V_{o,pl,Rd} = \left[ V_{pl,Rd} - \frac{d_o t_w f_{yd}}{\sqrt{3}} \right] \quad (9)$$

Where the shear resistance,  $V_{pl,Rd}$ , for un-perforated beams EC3 EN1993-1-5 [35] is limited by either the plastic shear resistance:

$$V_{pl,Rd} = \frac{A_v \left( \frac{f_y}{\sqrt{3}} \right)}{\gamma_{Mo}} \quad (10)$$

Where  $A_v$  is taken as  $A_v = A - 2b_f t_f + (t_w + r)t_f$ , and the value of  $\gamma_{Mo}$  is equal to 1.

Comparing the FE results with the results obtained from the theoretical formulae given above, it is found that:

- The basic shear capacity approach given by Chung et al. [16] for steel perforated beams is the closest approach to the FE analyses, with an average deviation ( $F_{theory}/F_{FE}$ ) ratio of 0.93.

- The shear resistance approaches given by Lawson and Hicks [36] **Eq. 7** and **8**, slightly underestimate the results compared to the FE analyses, with average deviation ratios of 0.90 and 0.86, respectively. The most effective approach is when the shear resistance is limited by the plastic shear resistance for the un-perforated section (**Eq. 7**).

The comparison leads to the following conclusions:

- The smaller the degree of shear connection,  $\beta$ , used in the FE models, the greater the deviation ratio is.
- For steel grade S275, the FE results are closer to the theoretical design values. In contrast, when steel grade S355 is used, the FE results obtained are overestimated because of the increased stiffness of the FE model with solid elements.

## 7. Conclusions

The USFB offers lower structural depth inversely to conventional composite beams, where the concrete slab sits on top of the plain (or perforated) steel beam. The decrease of the structural depth for every floor, and the ease of construction for large spans, as heavy propping is not needed, makes USFBs worth studying. Although the capacity of the perforated beam is reduced by using large web openings ( $d_o=0.76h$ ), the designer can take advantage of the inherent double shear strength provided by the confined concrete between the flanges and the bearing plates at the supports. Hence, increased flexural strength of the composite beams as well as longitudinal shear strength due to the concrete passing throughout the web openings is achieved.

The following conclusions can be drawn from this study:

- With the concrete in-fill, the ultimate vertical load carrying capacity of the USFB increases by up to 108% (i.e. double the capacity) compared to the corresponding non-composite perforated steel beam. This percentage is higher when the friction coefficient is closer to 1.0 (i.e. fully bonded). It is assumed that there will be a lower concrete contribution if bearing plates are not provided at the supports.
- All four experimentally tested USFBs showed consistent behaviour in terms of the failure mode, stiffness and the ultimate load carrying capacity.
- The failure mode of the non-composite beam changes when there is in-filled concrete between the flanges.
- The concrete failed first before any significant distortion of the steel web occurs.

- The last descending post-elastic branch of the load-deflection curve corresponds to the composite beam behaviour as a 'mechanism'. Failure is accompanied with the appearance of wide diagonal concrete crushing.
- Following the formation of large diagonal cracks, there is some residual strength in the concrete preventing local buckling of the perforated steel beams and the load carrying capacity is somewhat higher than that on the non-composite beam.
- The shear resistance of the USFB, without using any mechanical shear connectors, is provided mainly of contributions from the concrete confinement and the steel flange thickness.
- Strut action of the concrete confinement across the web openings reduces the Vierendeel bending effects and improves the vertical shear transfer in the vicinity of the web openings. Hence, the vertical shear force resisted by the concrete at a web opening is dependent on the on the flange dimensions.
- The horizontal component of the strut action is dependent on the frictional force, shear-bond resistance and the bearing strength of the web opening area.

In order to study the parameters affecting the structural behaviour of simply supported USFBs with larger circular web openings, three-dimensional finite element models employing solid elements were developed. The FE results are summarised below:

- The FE models accurately simulate the structural behaviour of the USFBs tested up to the ultimate load carrying capacity level. Comparison between the measured and the predicted load carrying capacities against the Vierendeel mechanism was found to be close.
- Various constitutive relationships modelling the concrete material properties were found from the sensitivity-parametric studies to affect the load carrying capacity of USFBs differently.
- As the composite beams examined did not contain confined reinforcement, the concrete tensile strength played a major role in defining the divergence load.
- All cracks in the FE models develop at a higher load compared to those observed in the experiments.
- A design method for simply supported conventional un-perforated composite beams presented by Liang et al. [24] was modified for the shear resistance of the both perforated sections and simply supported USFBs with any degree of shear connection between the steel and the concrete. The results compared well with those from the FE analyses.
- Overall, it is shown that the FE models not only provide quantitative justification as to the structural adequacy of the proposed design method, but also provide advanced computational-based analytical and design tools for the detailed structural behaviour of USFBs.

## Acknowledgements

The results from this research study are incorporated in ASD Westok's Ltd. (2010) design software for USFBs (USFB-AutoMate v1.0) developed and certified by the Steel Construction Institute (SCI). The authors would like to thank the ASD Westok group for the supply of the steel perforated specimens and the SCI for the approval of the experimental setup, structural arrangements and geometrical configurations of the specimens.

## Abbreviations

$A_{ec}$	Effective shear area of concrete
$b_f$	Width of the top flange of steel beam
CSR	Specification of the Cohesion Sliding Resistance
$d_o$	Web opening diameter
$h$	Overall depth of the steel beam
$P_{con}$	Contact pressure
$r$	Root radius of steel UB section
$t_f$	Flange thickness
$t_w$	Web thickness
$V_c$	Nominal shear strength (contribution of the concrete to the vertical shear strength)
$V_o$	Shear strength of the beam in pure shear (with zero degree of shear connection)
$V_s$	Shear capacity of the web of the steel beam to the vertical shear strength
$V_{uo}$	Ultimate shear strength of the composite beam in pure shear
$\mu$	Coefficient of friction
$\beta$	Degree of shear connection at a cross-section

## References

- [1]De Nardin S, El Debs ALHC. Study of partially encased composite beams with innovative position of stud bolts. Journal of Constructional Steel Research 2009; 65:342-350.
- [2]Bernuzzi C, Zandonini R. In: Buckner, D. and Shahrooz, B.M. editors. Slim floor steel-concrete composite systems, Composite construction in steel and concrete, vol. III. Germany: ASCE 1996; 486-99.
- [3]Viest IM, Colaco JP. Composite construction design for buildings. ASCE, Reston, Va., 1997.
- [4]Hegger J, Goralski C. Structural behaviour of partially concrete encased composite sections with high strength concrete. 5<sup>th</sup> International conference in composite construction in steel and concrete, South Africa, 2005; 346-55.

- [5]Dipaola V, Prete F, Prete G. The elasto-plastic behaviour of encased composite beams for slim floors in multi-storey buildings. 2<sup>nd</sup> International congress-Fib, Naples, FIB, 2006; (ID 5-24):1-12.
- [6]Wang Y, Yang L, Shi Y, Zhang R. Loading capacity of composite slim frame beams. Journal of Steel Constructional Research 2009; 65:650-661.
- [7]Ju YK, Chun SC, Kim SD. Flexural test of a composite beam using asymmetric steel section with web openings. Journal of Structural Engineering ASCE 2009; 448-458.
- [8]ASD Westok Ltd. "<http://www.asdwestok.co.uk/Applications/Ultra+Shallow/>" 2011.
- [9]Hicks S. Current trend in modern floor construction. The Steel Construction Institute 2003; (11)1:32-32.
- [10]Tsavdaridis KD, Giaralis A. Derivation of Dynamic Properties of Steel Perforated Ultra Shallow Floor Beams (USFB) via Finite Element Modal Analysis and Experimental Verification. 7<sup>th</sup> National Conference on Steel Structures, Volos, Greece 2011; (053)2:321-329.
- [11]Tsavdaridis KD, D'Mello C. Optimisation of Novel Elliptically-Based Web Opening Shapes of Perforated Steel Beams. The Journal of Constructional Steel Research, 2011, accepted.
- [12]Tsavdaridis KD. Failure modes of composite and non-composite perforated steel beams sections with various shapes and sizes of web openings. PhD thesis (supervised by Dr. C. D'Mello), School of Engineering and Mathematical Sciences, City University, London, 2010.
- [13]BS EN197:Part 1:2000. Cement. Composition, specifications and conformity criteria for common cements, BSI, 2000.
- [14]BRE Design of normal concrete mixes, BRE report, UK, 1988.
- [15]Tsavdaridis KD, D'Mello C. Vierendeel Bending Study of Perforated Steel Beams with Various Novel Shapes of Web Openings, through Non-linear Finite Element Analyses. The Journal of Structural Engineering-ASCE, 2011, in revision.
- [16]Chung KF, Liu TCH, Ko ACH. Steel beams with large web openings of various shapes and sizes: an empirical design method using a generalized moment-shear interaction. Journal of Constructional Steel Research 2003; 59:1117-1200.
- [17]BS EN1994-1-1:2004 Eurocode 4. Design of composite steel and concrete structures. General rules and rules for buildings, BSI, 2004.
- [18]Yu Huo B, D'Mello C, Tsavdaridis KD. Experimental Study and Analytical Study of Push-out Shear Tests in Ultra Shallow Floor Beams. 34<sup>th</sup> IABSE Symposium, Venice, Italy 2010, IABSE Press, pp. 31-38.

- [19] Lawson M. Enhanced Design of Ultra Shallow Floor Beams. Technical Paper in New Steel Construction (NSC) Magazine, June, 2011.
- [20] Shayanfar MA, Kheyroddin A, Mirza M.S. Element size effects in nonlinear analysis of reinforced concrete members. Computers & Structures 1997; (62)2:339-352.
- [21] Choi CK, Kwak HG. The effect of finite element mesh size in nonlinear analysis of reinforced concrete structures. Computers & Structures 1990; (36)5:807-815.
- [22] Tsavdaridis KD, D'Mello C, Huo BY. Shear Capacity of Perforated Concrete-Steel Ultra Shallow Floor Beams (USFB). 16<sup>th</sup> National Concrete Conference, Paphos, Cyprus 2009; Ref no: 201101, 159.
- [23] Tsavdaridis KD, D'Mello C, Hawes M. Experimental Study of Ultra Shallow Floor Beams (USFB) with Perforated Steel Sections. Nordic Steel Construction Conference - NSCC2009, Malmö, Sweden 2009, Ref. no:128, 312-319.
- [24] Liang QQ, Uy B, Bradford MA, Ronagh HR. Strength analysis of steel-concrete composite beams in combined bending and shear. The Journal of Structural Engineering-ASCE 2005; (131)10: 1593-1600.
- [25] William KJ, Warnke EP. Constitutive model for triaxial behaviour of concrete. International Association of Bridge and Structural Engineering Conference, Bergamo, Italy 1974, ISMES Press; 19, 174.
- [26] Kachlakev, Miller T. FE Modeling of Reinforced Concrete Structures Strengthened with FRP Laminates. Final Report SPR 316, Oregon State University, Department of Transportation, 2001.
- [27] Kaewunruen S, Remennikov A. Nonlinear finite element modelling of railway prestressed concrete sleeper, 10<sup>th</sup> East Asia-Pacific Conference on Structural Engineering and Construction - Real Structures: Bridges and Tall Buildings. Bangkok, Thailand 2006; 4:323-328.
- [28] Parvanova SP, Kazakov KS, Kerelezova IG, Gospodinov GK, Nielsen MP. Modelling the nonlinear behaviour of R/C beams with moderate shear span and without stirrups using ANSYS. Faculty of Civil Engineering, Sofia, Research for the National Science Fund under the contract № TH-1406/04, Technical Report, 2004.
- [29] Bangash MYH. Concrete and concrete structures: Numerical modelling and applications Elsevier Applied Science (London and New York), Book (ISBN 1851662944 ) 1989; PUB I:102-796-517.
- [30] ACI Committee 318: Building Code Requirements for Reinforced Concrete. Detroit. American Concrete Institute. 1999.
- [31] AS3600: Concrete Structures Standard. Standards Association of Australia, 2009.
- [32] BS 8110-1:1997. Structural use of concrete, Code of practice for design and construction, BSI, 1997.

[33]Buckhouse ER. External Flexural Reinforcement of Existing Reinforced Concrete Beams using Bolted Steel Channels. Master's Thesis, Marquette University, Milwaukee, Wisconsin, 1997.

[34]Rust W, Schweizerhof K. Finite element limit load analysis of thin-walled structures by ANSYS (implicit), LS-DYNA (explicit) and in Combination. Copyright 2002 Elsevier Science Ltd., Thin Walled Structures, 2003; (41)2-3:227-244.

[35]EC3 EN1993-1-5: Design of steel structures – General rules; Supplementary rules for planar plated structures without transverse loading, 1993.

[36]Lawson RM, Hicks SJ. Design of beams with large openings for services. Steel Construction Institute 2006; P-355.